Measurement of higher-order harmonic flow in PbPb collisions at center-of-mass energy = 2.76 TeV

CMS Collaboration
(Dated: January 20, 2013)

We report on the measurements by the CMS experiment of higher-order flow anisotropy harmonic coefficients for $\sqrt{s_{NN}}$ = 2.76 TeV PbPb collisions at the LHC. Expressed in terms of a Fourier decomposition of the azimuthal distribution with respect to a global event plane related to the shape of the overlap region, the n=3,4, and 5 coefficients (corresponding to the v_3 through v_5 hydrodynamic flow parameters) in the expansion are presented as a function of transverse momentum (p_T), collision centrality (0-70% most central events) and pseudorapidity ($|\eta| < 2.0$). The analysis is done using the event plane, cumulant, and Lee-Yang Zero methods, allowing for the role of participant fluctuations and nonflow correlations to be explored by the different sensitivities of these methods to these effects. In general, the odd harmonics are found to be much less sensitive to collision centrality than the even harmonics, as would be expected if the odd harmonics are dominated by fluctuation effects. The yield-weighted average flow coefficients show a weak dependence on pseudorapdity, reaching their maximum values at mid-rapidity. Taken together with earlier LHC measurements of elliptic flow (v_2), these results help develop a more complete picture of the collective motion that develops in high-energy, heavy-ion collisions and help to define the properties of the produced medium.

I. INTRODUCTION

In the collision of two heavy ions moving at relativistic speeds, a region of high-energy-density matter is created in the overlap region of the two Lorentz contracted nuclei. Earlier studies of the medium modification and azimuthal anisotropy and of emmitted particles at RHIC, where gold nuclei were collided at nucleon-nucleon center-of-mass energies up to $\sqrt{s_{NN}}$ = 200 GeV [1–4], have been interpreted in terms of the creation of a strongly interacting quark-gluon plasma state of matter. The created medium is found to behave as a near perfect fluid with a transverse viscosity to entropy ratio (η/s) approaching the conjectured lower limit for this quantity [5–8]. Presure gradients that develop in the fluid during the collision lead to an anisotropic momentum distribution of the outflowing matter which, in turns, leads to a preferential emision of particles in the short direction of the lenticular shaped overlap region [9–11]. The hydrodynamic behavior suggests that local thermal equilibrium may be achieved very rapidly through the scattering of partons in the initial hot medium, with the observed anisotropy in particle emission then being sensitive to the basic properies of the created medium, including its equation of state, the η/s value, the speed of sound in the medium (c_s), and initial conditions such as whether the collision developes through a Glauber-like picture of individual nucleon collisions [12], or whether gluon saturation effects as found in the Color Glass Condenstate model [13] play an important role.

More recently, the azimuthal anisotropy measurements have been extended to a much higher collision energy, with PbPb collisions at $\sqrt{s_{NN}}$ = 2.76 TeV [14–16] studied at the LHC. Moreover, the azimuthal behavior is being developed with greater precision with the exploration of higher-harmonic components of the behavior at both the RHIC [17–21] and the LHC [22–24] facilities. The azimuthal dependence of the particle yield can be written in terms of an harmonic expansion with [25]

$$E\frac{d^3N}{d^3p} = \frac{1}{2\pi}\frac{d^2N}{p_T dp_T dy}\left(1+\sum_{n=1}^{\infty}2v_n\cos\left[n\left(\varphi-\Psi\right)\right]\right) \quad (1)$$

where φ, E and p_T are the particle's azimuthal angle, energy, and transverse momentum, respectively. If the impact-parameter direction is known, the reference angle Ψ can be taken as the azimuthal angle of the reaction plane Ψ_R as defined by the beam and impact parameter directions. In analyzing an experimental distribution, the reference direction needs to be determined in terms of the observed event-by-event global azimuthal asymmetry of particle emission. The higher-harmonic behavior is particulary sensitive to fluctuations in the initial conditions [26–39] and to the shear viscosity of the created medium [29, 40–43].

This paper presents the results from the CMS collaboration on higher-harmonic flow components for PbPb collisions at $\sqrt{s_{NN}}$ = 2.76 TeV. To better understand the role of initial-state fluctuations and non-flow behaviors on the observed azimuthal distributions, the data are analyzed using the event-plane, cumulant, and Lee-Yang Zeros methods to exploit the different sensitivities of these methods to these effects. This work extends the previously published CMS results on elliptic flow (the n=2 harmonic) [16]. The data and event selection used here are identical to that used in the elliptic flow analysis and the current discussion of the experimental method summarizes a more extensive discussion presented in the earlier paper. New results are presented for the n=3,4 and 5 harmonics as a function of transverse momentum ($0.3 \leq p_{\mathrm{T}} < 8.0\,\mathrm{GeV}/c$), centrality (0–70%), and pseudorapidity ($|\eta| < 2.0$). Some of the earlier elliptic flow results are included to help develop the harmonic systematics. CMS has also measured higher-harmonic

anisotropies with $1.0 \leq p_{\rm T} < 20$ GeV/c using the two-particle correlation method [44]. These results are also included here for comparison.

The paper is organized as follows. Section II presents an overview of the experimental proceedures and discussions of the different methods that were used in the analysis. The systematic uncertainties for the different methods are presented. This section also develops the Glauber-model calculations used to obtain the eccentricities employed in discussing the experimental results. Section III presents the differential and spectrum-weighted integral harmonic coefficients for the different methods. For the comparison plots we also include previously published two-particle correlation results obtained by the CMS collaboration. The pseudorapidity dependence is presented for the event-plane method. Section III also contains a comparison of the new CMS results to previously published results of the ALICE and ATLAS collaboration. Section IV presents a discussion of the results. We conclude in Section V with a summary of our results.

II. EXPERIMENTAL DETAILS

The measurement was done with the Compact Muon Solenoid (CMS) detector using $\sqrt{s_{NN}} = 2.73$ GeV Pb+Pb data obtained during the Fall, 2010 heavy-ion run at the Large Hadron Collider. This section discusses the details of event selection, the tracking efficiency and fake track corrections, the three analysis methods used in determining the harmonic flow coefficient, and the systematic uncertainties associated with the measurements. The analysis uses the same data and techniques as for the elliptic flow study of ref. [16], allowing for a direct comparison with the results of that study.

A. Tracking and Centrality

The Compact Muon Solenoid (CMS) apparatus consists of a silicon tracker, a crystal electromagnetic calorimeter, and a brass / scintillator hadronic calorimeter housed within a 6 m diameter superconducting solenoid, providing a 3.8T magnetic field. Outside of the solenoid, muons are measured in gas-ionization chambers that are embedded in a steel return yoke. Additionally, the CMS detector includes extensive forward calorimetery. The inner tracker consists of silicon pixel and strip detector modules, and reconstructs charged particles within the pseudorapidity range $|\eta| < 2.4$. In the forward region, two steel/quartz-fiber Čerenkov Hadron Forward (HF) calorimeters cover a pseudorapidity range of $2.9 < |\eta| < 5.2$, and are azimuthally subdivided into 20° modular wedges. the Beam Scintillation Counters (BSC) are scintillator tiles placed along the beamline at distances of $\pm$10.9 m and $\pm 14.4m$ from the interaction point. The BSC detectors can provide hit and coincidence rates and are sensitive to almost the full PbPb interaction. A more detailed description of the CMS detector can be found elsewhere [45]. In this analysis, the azimuthal flow correlations were determined based on the charged particles leaving trackins in the Si tracker detector. The event-plane anlysis also uses information from the HF calorimetors to establish event planes that were far removed in pseudorapidity from the tracks used to determine the flow harmonics.

From the 2010 heavy-ion run of the LHC, minimum bias PbPb events were triggered by coincident signals from both ends of the CMS detector in either the BSC or HF. This trigger is required to be in coincidence with the presence of both colliding ion bunches in the interaction region. Additional offline event selections were applied in order to obtain a pure sample of inelastic hadronic collisions, which removed contamination from non-collision beam backgrounds and from ultraperipheral (UPC) collisions where an electromagnetic interaction leads to the breakup of one or both Pb nuclei [46]. These offline selections included the requirement of proper timing of the BSC signals from both sides of the detector, a coincidence of three HF towers on either side of the interaction point, a reconstructed vertex compatible with the expected collision region, and the shape of reconstructed clusters from the pixel detector being compatible with being produced by particles originating from the primary collision vertex.

Events used in this analysis were required to have a longitudinal vertex position within 10 cm of the geometric center of the detector in order to consistently measure charged particle distributions at forward rapidity. After all selections, 22.6 million events remained in the final sample, corresponding to an integrated luminosity of approximately 3 μb^{-1}. This final sample is the same data set used in the elliptic flow study where it is described in further detail [16].

The centrality of a collision is a measure of the degree of overlap of the colliding ions. Several observables depend on the centrality and can be used for its determination. In this analysis, the total energy deposited in both HF calorimeters was used, with the distribution of the total energy for all events divided into 40 centrality bins, each representing 2.5% of the total PbPb interaction cross section. These bins were then combined to form the final 5% or 10% bins used to present the final results. The measured charged particle multiplicity distribution does not represent that from the full interaction cross section due to inefficiencies in the minimum bias trigger and the event selection. Monte Carlo (MC) simulations were used to estimate the multiplicity distribution in the regions where events are lost. Comparing the simulated distribution to the measured distribution, we measure the combined efficiency for the minimum bias trigger and the event selection to be $(97 \pm 3)\%$.

Track reconstruction is accomplished by starting with a set of three reconstructed signals in the inner layers of the silicon pixel detector that are compatible with a helical trajectory with some minimum $p_{\rm T}$ in some selected region around the reconstructed primary collision

vertex. This process is performed in two iterations. In the first iteration, trajectories with a minimum $p_{\rm T}$ of 1.5 GeV/c are propagated outward through subsequent silicon strip layers using a combinatorial Kalman filter algorithm [47]. In the second iteration, trajectories in the range of $0.3 < p_{\rm T} < 1.8$ GeV/c are determined from only signals in the pixel detector, and are not propagated outward through the silicon strip detector layers. The reconstructed tracks from both iterations are then merged into a single collection, removing duplicate tracks by using the reconstructed signals in common to both tracks, and giving preference to the first-iteration tracks. This track reconstruction method is identical to that used in the elliptic flow analysis where it is described in greater detail [16].

At low-$p_{\rm T}$ the fraction of misreconstructed or "fake" tracks is significant, and in this kinematic region the v_n signal is small. Studies using a full CMS MC simulation based on the HYDJET [48] and AMPT [49] event generators have indicated that the v_n signal of fake tracks is approximately constant for $p_{\rm T} < 0.8$ GeV/c. These fake tracks may then carry a much larger v_n signal at low-$p_{\rm T}$ than the properly reconstructed tracks, and significantly distort the measured v_n signal. Therefore, it is necessary to correct for this influence in the range $p_{\rm T} < 1.0$ where it may be significant. Both empiricial studies and MC simulations have indicated that the v_n of fake tracks may be characterized as $v_n^{\rm fake} = \alpha \langle v_n \rangle$, where the yield-weighted average $\langle v_n \rangle$ is performed over the transverse momentum range 0.3 to 3 GeV/c folding in the efficiency-corrected spectra, and α is an empirically determined scaling factor. The value of α is dependent on the harmonic, and was found to be 1.3 ± 0.1 for v_2, 1.0 ± 0.4 for v_3, and 0.8 ± 0.6 for all higher harmonics.

Letting f represent the proportion of fake tracks, the observed v_n distorted by the influence of the fake tracks, $v_n^{\rm obs}$, is related to the flow signal of just the properly reconstructed tracks, $v_n^{\rm real}$, by the equation:

$$v_n^{\rm obs} = (1-f) v_n^{\rm real} + f v_n^{\rm fake} \quad (2)$$

From this equation, and using the understanding of $v_n^{\rm fake}$, the final measured v_n signal has been corrected to remove the influence of the misreconstructed tracks.

B. Analysis Methods

Anisotropic flow is formed by the azimuthal correlation of produced particles with respect to the participant plane of a heavy-ion collision. This induces correlations between the particles emitted from the collision zone. In addition to correlations due to flow, there exist other sources of azimuthal correlations, such as the correlations from resonance decay and jets that do not depend on the reaction plane orientation. These type of correlations are called non-flow correlations. To measure the "true" flow, we must remove or lessen non-flow correlations. To extract v_n, the event plane [25], cumulant [50, 51] and the Lee-Yang zeros [52, 53] methods are used. The event-plane method measures correlations with an "event-plane angle" $\Psi_{\rm m}$ of a given order m that is determined in a different pseudorapdity window from where the v_n coefficients are being measured. The cumulant and Lee-Yang zeros methods are both based on correlations between multiple particles in the event. In these two methods, an integral flow generating function is first produced in terms of a given harmonic v_m. This generating function plays a similar role to that of the event-plane determination in the event-plane method. Based on the integral generating function, it is possible to determine the "differential" flow harmonics $v_{\rm n}(p_T)$. In each of the three methods, the differential harmonic expansion coefficients $v_{\rm n}(p_T)$ can be determined with respect to the fundamental harmonic m, where n is an integer multiple of m. Thus, we can use m=2, the harmonic with the greated amplitude, for the order of the event-plane angle or integrated flow to reconstruct any even harmonic v_{km}, with n = km and k=1,2,3, etc. However, fluctuations of the participant locations will, in general, lead to different values of $v_{\rm n}$ for different k and m combinations. Limited event multiplicity generally restrict the determination of differential $v_{\rm n}(p_T)$ values for n odd in the cumulant and Lee-Yang zeros methods to the same order as the fundamental harmonic used for the generating function. Additionally, the measurement of any harmonic in both the cumulant and Lee-Yang zeros methods is dependent on the magnitude of the resolution parameter $\chi \equiv v_m\sqrt{M}$, where v_m is the harmonic used for integrated flow and M is the multiplcity. Typically, v_m is too small in central collisions and M is too low in peripheral collisions to extract orders of differential v_n higher than the lowest order ("m") in the cumulant method or Lee-Yang zeros methods.

1. *Event-plane Method*

The event-plane method [25] measures flow with respect to an event plane angle of a given order m that is determined in a different pseudorapidity region from that for which the flow coefficient is being measured. Expressed in terms of the event-plane angle corresponding to harmonic m, the expansion of the azimuthal behavior becomes

$$E\frac{d^3N}{d^3p} = \frac{1}{2\pi}\frac{d^2N}{p_t dp_t dy}\left(1 + \sum_{k=1}^{\infty} 2{\rm v}_{km}^{obs}\cos\left[km\left(\phi - \Psi_{m,EP}\right)\right]\right), \quad (3)$$

where n = km. Using the first-order, m=1 event plane, all interger values of n (=k) are possible. More commonly, the expansion is done using the second-order, m=2 event plane. In this case, only even terms are included in the

expansion. Generally, when higher order event planes are considered ($m > 2$), only the $k = 1$ term is kept.

The method assumes that the event-plane angle is a pseudorapdity-independent global observable. For this analysis, event-plane angles are calculated using the transverse energy measurements of elements of the azimuthally symmetric forward CMS hadronic calorimeters (HF), with

$$\Psi_m = \frac{1}{m}\tan^{-1}\left\{\frac{\langle w_i \sin(m\phi_i)\rangle}{\langle w_i \cos(m\phi_i)\rangle}\right\}. \quad (4)$$

The HF calorimeters are azimuthally subdivided into 20 deg modular wedges, and segmented to form $0.175 \times 0.175(\Delta\eta \times \Delta\phi)$ towers. The bracket ($\langle\rangle$) indicates a sum over tower elements, with each tower weighted by the its correponding transverse energy. For each fundamental harmonic m we define two event planes Ψ_m(HF$-$) ($-5 < \eta < -3$) and Ψ_m(HF+) ($3 < \eta < 5$), corresponding to the HF calorimeters on either side of the nominal vertex location. A standard event-plane flattening procedure was employed to avoid having an azimuthal bias introduced by detector effects [16, 25]. The differental flow parameters $v_{p_T,\eta}$ are then determined with

$$v_n^{obs}(p_T, \eta < 0) = \ll \cos[n\{(\phi - \Psi_m(\mathrm{HF}+))\}] \gg \quad (5)$$

and

$$v_n^{obs}(p_T, \eta > 0) = \ll \cos[n\{(\phi - \Psi_m(\mathrm{HF}-))\}] \gg, \quad (6)$$

where $\ll\gg$ indicates first taking a sum over all particles in an event with a given Ψ_m, and then a sum over all events. Here ϕ is the azimuthal of a particle of pseudorapidity η. Particles with $\eta < 0$ are correlated with HF+, and those with $\eta > 0$ are correlated with HF$-$. In this manner, a minimum psuedorapdity gap of 3 units is maintained between any particle used in the event-plane angle determination and that being used to determine the flow harmonic.

Figure 1 illustrates how eqn. 3 relates to actual experimental results. The azimuthal distribution of tracks with $0.3 \le p_T < 2.6$ GeV/c for the 0-5% and 30-35% centrality ranges near mid-rapidity are shown with respect to the m=2,3,4 and 5 harmonic event planes. The *same* data are used for the distributions in each of the four panels. The distributions are shown for the angular ranges appropriate for the different harmonics (i.e., $|\phi - \Psi_m^{\mathrm{EP}}| \le \frac{\pi}{m}$) with $0.3 \le p_T < 2.6$ GeV/c and for the 0-5% (closed circles) and 30-35% (open circles) centrality ranges. In each case, the expermental distributions are fitted with leading-order terms of eqn. 3. For all but the m=2, 30-35% distribution, the experimental results are well described by the lowest (k=1) term in the expansion. The first two term (k=1 and k=2) are needed for a good description of the m=2, 30-35% distribution. It should be noted that there can be a significant difference in a given flow harmonic v_n depending on the order m of the event plane used in its determination.

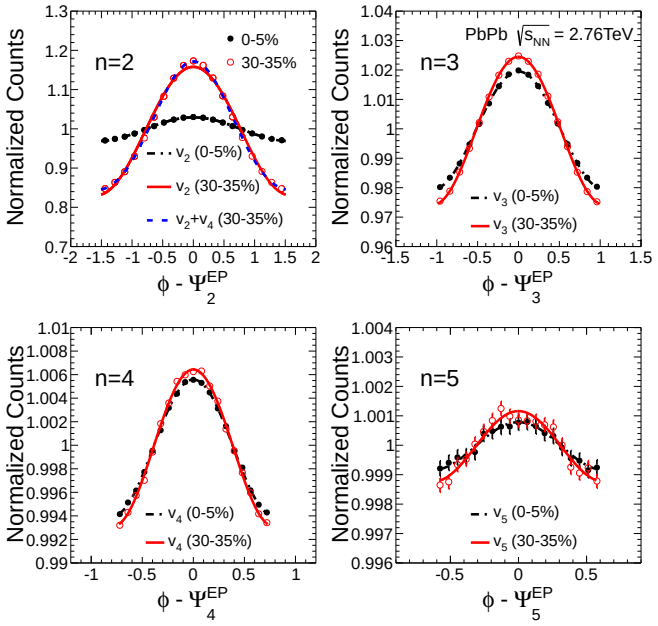

FIG. 1. (Color online) Charged-particle azimuthal distributions with respect to event planes of order m=2,3,4 and 5. The data are shown for two centrality ranges (0-5% and 30-35%) and correspond to tracks measured with $0.3 \le p_T < 2.6$ GeV/c in the pseudorapidity range $|\eta| < 0.8$.

The observed flow value v_n^{obs} will depend on the resolution of the event-plane angles and is therefore sensitive to both the particle multiplicity and the fundamental flow harmonic in the pseudorapidity range covered used to determine the event-plane angle. The final flow values are corrected for the event-plane angle resolution correction factor $R_n\{\Psi_m\}$, with $v_n\{\Psi_m\} = v_n^{obs}\{\Psi_m\}/R_n\{\Psi_m\}$. To determine $R_n\{\Psi_m\}$ we use the three-subevent method [25] where the resolution of Ψ_m^a associated with subevent a (e.g., HF$-$) is determined using additional seperate subevent angles Ψ_m^b (e.g., HF+) and Ψ_m^c, with

$$R_n^a\{\Psi_m\} = \sqrt{\frac{\langle\cos[n(\Psi_m^a - \Psi_m^b)]\rangle\,\langle\cos[n(\Psi_m^a - \Psi_m^c)]\rangle}{\langle\cos[n(\Psi_m^b - \Psi_m^c)]\rangle}}. \quad (7)$$

For this analysis Ψ_m^c was determined using the CMS tracker detector and corresponded to particles emitted with $|\eta| < 0.75$. Here the weights used in Eq. 4 were the corresponding transverse momenta of the particles. The resolution correction values used in the analysis are shown in Fig. 2.

2. *Cumulant method*

The cumulant method measures flow utilizing a cumulant expansion of multiparticle azimuthal correlations, without determining the orientation of the event plane.

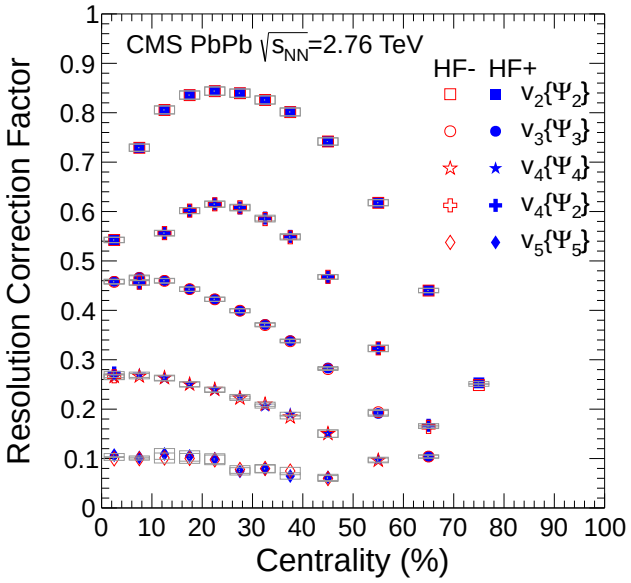

FIG. 2. (Color online) Event-plane resolution correction factors used in the analysis. For the second-order event plane (Ψ_2) the resolution correctons are shown for both the k=1 (n=2) and k=2 (n=4) harmonic terms of eqn. 3

The premise is that if the emitted particles are correlated with the event-plane orientation, then there also exist correlations between these particles. To calculate the cumulants of these correlations, from which the flow coefficient is extracted, a generating function of the multiparticle correlations in a complex plane [50, 51] is introduced. First, the reference flow is evaluated by constructing the corresponding generating function using all particles in a broad ($p_{\rm T}$, η) window, averaging over the events in a given centrality class. Then, the differential flow, i.e., the flow in a narrower phase-space window, is measured with respect to the reference flow. A particle in the differential bin is correlated to the particles used for the reference flow through a differential generating function. To avoid auto-correlations, if a given particle is used in determining the differential flow, the particle will be excluded in the calculation of the reference flow. The generating functions for the reference flow and for the differential flow are calculated at several different points in the complex plane and then interpolated. Three and two values for the radius parameter, r_0 were used for the reference flow and the differential flow respectively. Eight values for the polar angle were utilized for both of them. The radius parameters are determined according to the detected charged particle multiplicity and the number of events analyzed in each centrality class. To reduce the possible multiplicity fluctuation effect on flow measurements in a centrality interval, a fraction of particles in each event was selected at random to determine the reference flow. In the analysis, 80% of mean multiplicity ($\langle M \rangle$) was used. In addition, the transverse momentum restriction to $p_{\rm T} < 3$ GeV/c in the reference flow was imposed to reduce the nonflow contribution. In the analysis, v_3 is measured with 4-particle correlations which is denoted as $v_3\{4\}$. $v_4\{5\}$ corresponds to v_4 asymmetry calculated relative to the integral v_2 behavior via 5-particle correlations.

3. *Lee-Yang Zeros method*

The Lee-Yang zeros (LYZ) method [52, 53] studies directly the large-order behavior of the cumulant expansion of the azimuthal correlations, and is motivated by the idea that correlating a large number of particles is the most natural way of studying genuine collective motion in the expanding medium. This higher-order behavior is measured by finding the locations of the zeros of a complex function, which determine the integrated flow in the system. Charged particles with $0.3 < p_T < 12$ GeV/c and $|\eta| < 2.4$ are used to calculate the integrated flow. Details of the method can be found in [16]. The integrated v_2 behavior was used to extract the differential v_4 term, where we used the product generating function method in our analysis.

C. Systematic Uncertainties

The systematic uncertainties include those common to all methods, as well as method-specific ones. Since we are reporting the results on v_n values for non-identified charged hadrons, it is important to investigate the tracking efficiency as a function of particle species since protons, pions, and kaons may have different v_n. We apply a conservative 0.5% uncertainty independently of p_T, η, and centrality, the same value as was used in the v_2 measurement to account for this effect [16]. The sensitivity of the harmonic flow coefficients to the centrality calibration was evaluated by varying the trigger efficiency by $\pm$3%. The resulting uncertainty on v_n is of the order 1%, and is applied independently of $p_{\rm T}$ and centrality. The uncertainty in the efficiency corrections, which will only affect the yield-weighted average v_n values, was evaluated by determining the efficiency based on the HYDJET model and, separately, by embedding simulated pions into real data PbPb events. Although the two resulting efficiencies have differences, the uncertainty on the yield-weighted average v_n values is at most 0.5%. Fake tracks affect both the differential $v_n(p_{\rm T})$ results and the yield-weighted average v_n measurements. These are generally the largest contribution to the systematic uncertainty, especially at low $p_{\rm T}$ for the most central events. Different sets of kinematic cuts on the pixel tracks were used and the ratio of the results provided an estimate of the systematic uncertainty due to this source in different $p_{\rm T}$ ranges.

For the event-plane method, the uncertainty in the resolution correction value is generally small compared to

TABLE I. $v_3\{\Psi_3\}(p_t)$ systematics

Source	$\mathbf{p_T}$**(GeV/c)**	**Centrality**		
		0 - 10%	10 - 50%	50 - 70%
Particle Composition	All	0.5%	0.5%	0.5%
Centrality Det.	All	1.0%	1.0%	1.0%
Track cut	[0.3; 0.4]	20.0%	10.0%	10.0%
	[0.4; 0.8]	3.0%	2.0%	2.0%
	[0.8; 8.0]	1.0%	1.0%	1.0%
Resolution Correction	All	1.0%	1.0%	3.0%
Total	[0.3; 0.4]	20%	11%	11%
	[0.4; 0.8]	4%	3%	4%
	[0.8; 8.0]	2%	2%	4%

TABLE II. $v_4\{\Psi_4\}(p_t)$ systematics

Source	$\mathbf{p_T}$**(GeV/c)**	**Centrality**		
		0 - 10%	10 - 40%	40 - 60%
Particle Composition	All	0.5%	0.5%	0.5%
Centrality Det.	All	1.0%	1.0%	1.0%
Track cut	[0.3; 0.4]	80.0%	20.0%	20.0%
	[0.4; 0.8]	6.0%	4.0%	4.0%
	[0.8; 8.0]	1.0%	1.0%	1.0%
Resolution Correction	All	2.0%	2.0%	5.0%
Total	[0.3; 0.4]	80%	21%	21%
	[0.4; 0.8]	7%	5%	7%
	[0.8; 8.0]	3%	3%	6%

TABLE III. $v_4\{\Psi_2\}(p_t)$ systematics

Source	$\mathbf{p_T}$**(GeV/c)**	**Centrality**		
		0 - 10%	10 - 50%	50 - 70%
Particle Composition	All	0.5%	0.5%	0.5%
Centrality Det.	All	1.0%	1.0%	1.0%
Track cut	[0.3; 0.4]	80.0%	20.0%	20.0%
	[0.4; 0.8]	6.0%	4.0%	4.0%
	[0.8; 8.0]	2.0%	1.0%	1.0%
Resolution Correction	All	1.0%	1.0%	2.0%
Total	[0.3; 0.4]	80%	20%	21%
	[0.4; 0.8]	7%	5%	5%
	[0.8; 8.0]	3%	2%	3%

TABLE IV. $v_5\{\Psi_5\}(p_t)$ systematics

Source	$\mathbf{p_T}$**(GeV/c)**	**Centrality**		
		0 - 10%	10 - 40%	40 - 50%
Particle Composition	All	0.5%	0.5%	0.5%
Centrality Det.	All	1.0%	1.0%	1.0%
Track cut	[0.3; 0.4]	100.0%	40.0%	40.0%
	[0.4; 0.8]	20.0%	5.0%	5.0%
	[0.8; 8.0]	5.0%	3.0%	3.0%
Resolution Correction	All	3.0%	10.0%	10.0%
Total	[0.3; 0.4]	100%	42%	42%
	[0.4; 0.8]	21%	12%	12%
	[0.8; 8.0]	6%	11%	11%

the kinematic cut uncertainty and is primarily a consequence of its statistical significance. This is seen in Tables I to IV where the systematic uncertainties for the $v_n(p_{\rm T})$ values obtained using the event-plane method are presented. However, for the v_5 measurement using the event-plane measurement, the resolution correction uncertainly becomes comparable to that for the kinematic cut uncertainty. The various systematic uncertainties are take to be uncorrelation and added in quadrature in presenting the v_n coefficients.

In addition to the systematic terms common to all methods, the cumulant analyses are also influenced by the choice of the r_0 parameter and by the multiplicity fluctuations in the reference flow. Tables V and VI show the systematic uncertainties associated with the $v_3\{4\}$ and $v_4\{5\}$ results. The multiplicity fluctuations are found to be particularly significant for the $v_3\{4\}$ results.

The effect of multiplicity fluctuations was also studied for the Lee-Yang zeros method. Table VII shows the systematic uncertainties for the $v_4\{LYZ\}(p_t)$ results. In this case, the total uncertaintes, again found by adding the component uncertainties in quadrature, are dominated by the track cut uncertainties.

D. Glauber-model calculations

The Glauber model treats a nucleus-nucleus collision as an independent sequence of nucleon-nucleon collisions, see [12] and references therein. The model can be used to obtain spacial geometry anisotropy parameters that are expected to be reflected in the observed particle anistopties. The Glauber model assumes that the nucleons in a nucleus are distributed according to a Woods-Saxon

TABLE V. $v_3\{4\}(p_t)$ systematics

Source	$\mathbf{p_T}$**(GeV/c)**	**Centrality**	
		10 - 40%	40 - 60%
Particle Composition	All	0.5%	0.5%
Centrality Det.	All	1.0%	1.0%
Track cut	[0.3; 0.5]	10.0%	10.0%
	[0.5; 0.8]	5.0%	5.0%
	[0.8; 8.0]	2.0%	2.0%
Mult. fluct.	All	4.0%	5.0%
r_0	All	1.5%	1.5%
Total	[0.3; 0.5]	11%	12%
	[0.5; 0.8]	7%	8%
	[0.8; 8.0]	5%	6%

TABLE VI. $v_4\{5\}(p_t)$ systematics

Source	p_T(GeV/c)	Centrality		
		5 - 10%	10 - 40%	40 - 60%
Particle Composition	All	0.5%	0.5%	0.5%
Centrality Det.	All	1.0%	1.0%	1.0%
Track cut	[0.3; 0.5]	15.0%	5.0%	5.0%
	[0.5; 0.8]	10.0%	3.0%	3.0%
	[0.8; 8.0]	5.0%	1.0%	1.0%
Mult. fluct.	All	1.0%	2.0%	3.0%
r_0	All	0.5%	1.0%	1.0%
Total	[0.3; 0.5]	15%	6%	6%
	[0.5; 0.8]	11%	4%	5%
	[0.8; 8.0]	6%	3%	4%

TABLE VII. $v_4\{LYZ\}(p_t)$ systematics

Source	p_T(GeV/c)	Centrality		
		5 - 10%	10 - 40%	40 - 50%
Particle Composition	All	0.5%	0.5%	0.5%
Centrality Det.	All	1.0%	1.0%	1.0%
Track cut	[0.3; 0.5]	10.0%	6.5%	2.5%
	[0.5; 8.0]	2.5%	2.0%	1.0%
Mult. fluct.	All	0.1%	0.9%	2.0%
Total	[0.3; 0.5]	10%	7%	4%
	[0.5; 8.0]	3%	3%	3%

distribution:

$$\rho(r) = \frac{\rho_0(1 + wr^2/R^2)}{1 + e^{(r-R)/a}} \tag{8}$$

where ρ_0 corresponds to the nucleon density in the center of the nucleus, R corresponds to the nuclear radius, a to the skin depth and w characterizes deviations from a spherical shape. For the case of ^{208}Pb, the parameters utilized are $R = 6.62$ fm, $a = 0.546$ fm and $w = 0$. The model assumes that nucleons in each nucleus travel on straight-line trajectories through the colliding system and interact according to the inelastic nucleon-nucleon cross section, σ_{inel}^{NN}, as measured in p+p collisions. The value used for Pb+Pb collisions at $\sqrt{s_{_{NN}}} = 2.76$ TeV is taken as $\sigma_{inel}^{NN} = 64 \pm 5$ mb.

The spacial anisotropies are calculated with the location of each participant weighted by the harmonic order [36], with

$$\varepsilon_{n,m} = \frac{\langle r_\perp^n \cos\left[n\left(\phi - \Phi_m\right)\right]\rangle}{\langle r_\perp^2\rangle} \tag{9}$$

where, for a participant located at coordinates x,y in the transverse plane, $r_\perp = \sqrt{x^2 + y^2}$, $\phi = \arctan\left(y/x\right)$, and

$$\Phi_m = \frac{1}{m}\arctan\frac{\langle r_\perp^m \sin\left[m\phi\right]\rangle}{\langle r_\perp^m \cos\left[m\phi\right]\rangle} \tag{10}$$

is the azimuthal angle of the participant plane. The averages are taken over all of the participant nucleons. For $n = m$ we define $\varepsilon_n = \varepsilon_{n,n}$. With this definition, ε_n can only take positive values and represents the maximum asymmetry for each collision, independent of the initial impact parameter vector direction between the centers of the simulated nuclei. The PHOBOS collaboration has demonstated the common scaling bahavior achieved for the elliptic flow, v_2, coefficient in AuAu and CuCu collations at $\sqrt{s_{NN}} = 200$ GeV/c with the geometric eccentricity ε_n [27].

Table VIII lists the results for the average number of participants, $\langle N_{\rm part}\rangle$, and the root-mean-square evaluation of the participant spacial anisotropy, $\sqrt{\langle\epsilon_n^2\rangle}$ or $\sqrt{\langle\epsilon_{n,m}^2\rangle}$, and the respective errors for the centrality bins utilized in this analysis.

III. RESULTS

In this section we present the results for the higher-harmonic coefficients as well as the previously published elliptic flow (v_2) [16] and two-particle correlation results [44] from the CMS collaboration for completeness. The $p_{\rm T}$ dependence of the coeffients at midrapidity is presented first, comparing the results based on the different analysis methods. This is followed by the spectrum-weighted integral v_n results which are developed in terms of both their centrality and pseudorapity dependence. We complete the section with comparisons of the CMS results to previously published results of the ALICE [22, 23] and ATLAS collaborations [24].

A. $p_{\rm T}$ dependence at mid-rapidity.

Figure 3 shows the previously published results of the CMS collaboration on the elliptic flow v_2 coefficient for $|\eta| < 0.8$ based on the event plane $v_2\{\Psi_2\}$, four-particle cumulant $v_2\{4\}$, and Lee-Yang Zeros analysis $v_2\{LYZ\}$ from ref. [16], and the two-particle correlations results of ref. [44]. The event-plane analysis employed the same event selection and event-plane determination as used in the current, higher-harmonic ($n > 2$) analysis. The two-particle correlation method is similar to a two-particle cumulant analysis, although in this case without working with generating functions. If both particles are correlated with an event plane, they will also be correlated with each other. The method, as applied to LHC data, is described in detail in refs. [22, 44] is for charged particles located with $|\eta| < 2.5$ and with a pseudorapidity gap between the particles of $2 < |\eta| < 4$.

The event-plane and two-particle correlations results are found to be very similar, although with a systematically smaller value for the two-particle correlation results for all but the most periperal (70-80%) centrality range. This suggest similar sensitive to initial-state fluctions and non-flow effect of the current implementation of the two methods where a large pseudorapidity gap is required

TABLE VIII. Glauber-model participant $\sqrt{\langle\epsilon_n^2\rangle}$ eccentricities. The last column gives the 4^{th}-order eccentricities based on the 2^{nd}-order participant plane. Eccentricities are calculated using r^n weighting of participants.

Centrality (%)	$\langle\mathbf{N_{part}}\rangle$	$\sqrt{\langle\epsilon_2^2\rangle}$	$\sqrt{\langle\epsilon_3^2\rangle}$	$\sqrt{\langle\epsilon_4^2\rangle}$	$\sqrt{\langle\epsilon_5^2\rangle}$	$\sqrt{\langle\epsilon_{4,2}^2\rangle}$
0 - 5	382.77	0.084 ± 0.004	0.097 ± 0.003	0.114 ± 0.005	0.131 ± 0.006	0.081 ± 0.041
5 - 10	329.73	0.127 ± 0.007	0.129 ± 0.005	0.148 ± 0.005	0.169 ± 0.007	0.104 ± 0.064
10 - 15	281.48	0.175 ± 0.011	0.154 ± 0.006	0.174 ± 0.006	0.198 ± 0.008	0.123 ± 0.059
15 - 20	239.15	0.219 ± 0.016	0.177 ± 0.007	0.199 ± 0.007	0.225 ± 0.008	0.143 ± 0.049
20 - 25	202.22	0.262 ± 0.016	0.199 ± 0.008	0.225 ± 0.009	0.250 ± 0.009	0.165 ± 0.049
25 - 30	169.82	0.301 ± 0.019	0.221 ± 0.009	0.254 ± 0.010	0.277 ± 0.010	0.193 ± 0.038
30 - 35	141.30	0.339 ± 0.022	0.245 ± 0.010	0.284 ± 0.011	0.307 ± 0.011	0.221 ± 0.039
35 - 40	116.41	0.375 ± 0.022	0.268 ± 0.011	0.317 ± 0.013	0.337 ± 0.012	0.254 ± 0.041
40 - 50	85.17	0.429 ± 0.024	0.308 ± 0.013	0.370 ± 0.016	0.385 ± 0.016	0.307 ± 0.035
50 - 60	52.66	0.501 ± 0.026	0.366 ± 0.015	0.445 ± 0.020	0.454 ± 0.018	0.385 ± 0.039
60 - 70	29.85	0.581 ± 0.027	0.422 ± 0.016	0.520 ± 0.023	0.513 ± 0.018	0.466 ± 0.039
70 - 80	15.36	0.662 ± 0.026	0.460 ± 0.012	0.596 ± 0.026	0.559 ± 0.015	0.549 ± 0.035

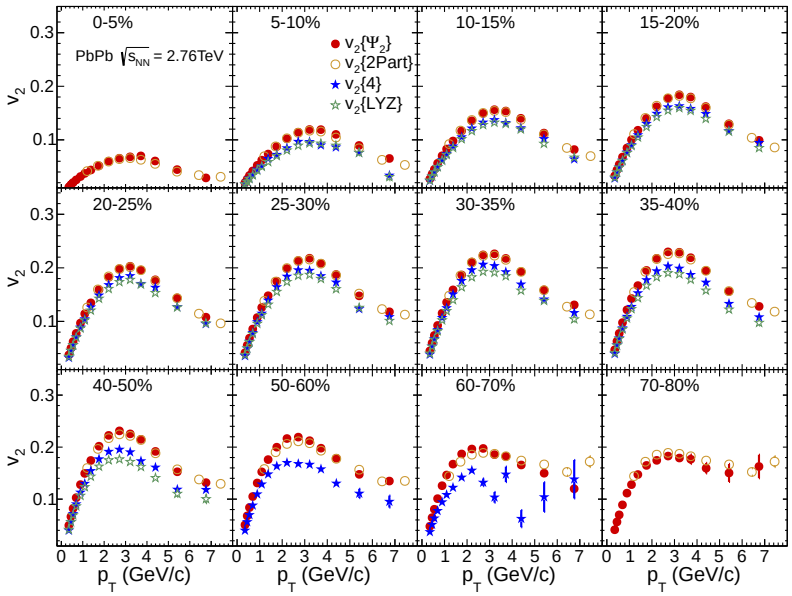

FIG. 3. (Color online) $v_2(p_T)$ values for event-plane $v_2\{\Psi_2\}$, two-particle correlations $v_2\{2\text{Part}\}$, four-particle cumulant $v_2\{4\}$ and Lee-Yang Zeros method $v_2\{\text{LYZ}\}$ methods. The $v_2(p_T)$, $v_2\{4\}$, and $v_2\{LYZ\}$ results are from ref. [16] and the $v_2\{2\text{Part}\}$ results are from ref. [44].

for both analyses. The slightly smaller values found for the two-particle correlationresults might result from this method sampling a larger pseudorapidity range then the event plane analysis which only considered particles with $|\eta| < 0.8$. The smaller values for the four-particle cumulant and Lee-Yang Zeros results for elliptic flow can be attributed to the reduced influence of eccentricity fluctuations and non-flow effects on these higher order correlations. This is described in detail in ref. [16]

The $n = 3$ azimuthal asymmetry results are shown in Fig. 4. The event-plane and two-particle correlations results are again found to be very similar to each other, with the event-plane angle found for the same harmonic as the studied azimuthal asymmetry, while the four-particle cumulant results are less than half the magnitude of the other two methods. This behavior is consistent with the odd-harmonic, $n = 3$ asymmetry being dominated by fluctuations in the initial state geometry as discussed in refs. [28, 36, 37, 54]

Figure 5 shows the v_4 values for a number of different methods. The event-plane results are shown based on both the 2^{nd}-order, elliptic flow event plane as well as the 4^{th} order event plane. A significant centrality dependence is observed for the $v_4\{\Psi_2\}$, $v_4\{5\}$, and $v_4\{\text{LYZ}\}$ results, while only a weak centrality dependence is found for the the $v_4\{\Psi_4\}$ and $v_4\{2\text{Part}\}$ values. The latter two

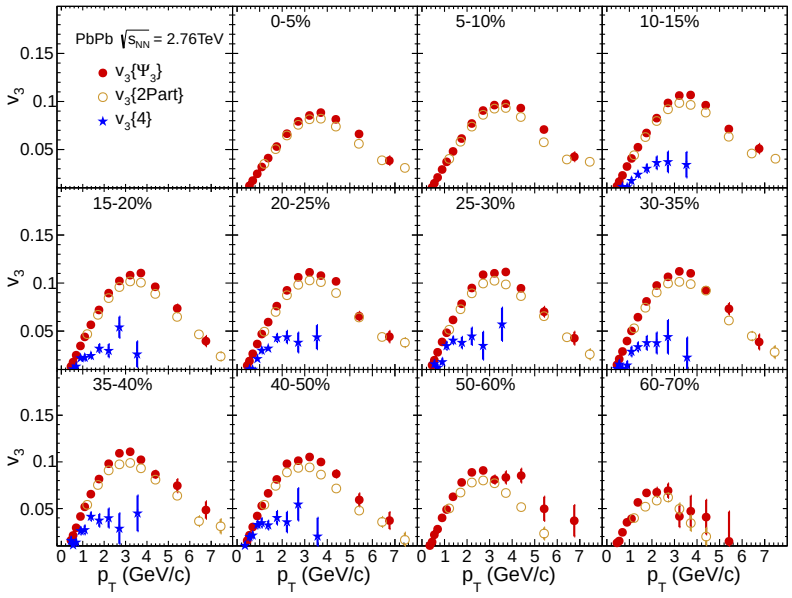

FIG. 4. (Color online) Azimuthal asymmetry v_3 coefficient for indicated methods.

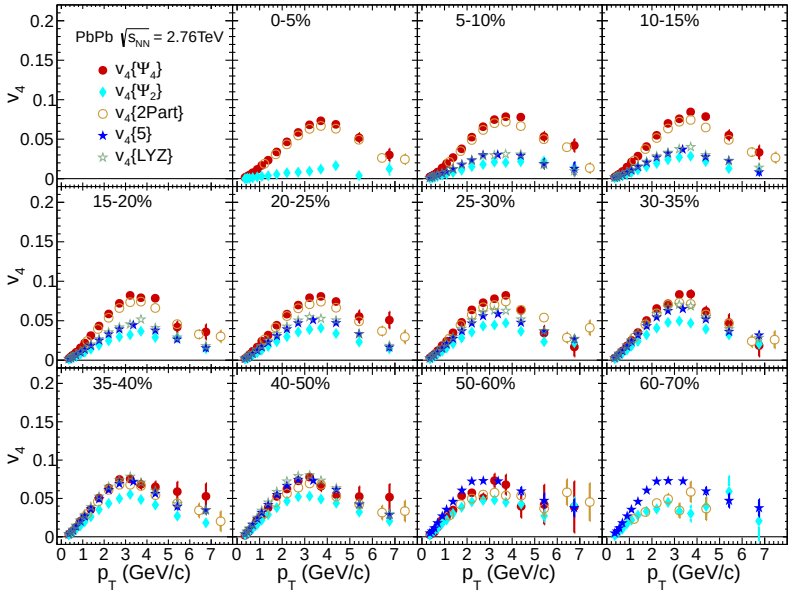

FIG. 5. (Color online) Azimuthal asymmetry v_4 coefficient for indicated methods.

methods again appear dominated by fluctuations of the initial state geometry over most of the centrality range.

Finally, figure 6 shows the v_5 asymmetry coeffients based on the event plane of the same $n = 5$ order and the two-particle correlation method. Similar to the other multipoles, the two methods give very similar results, with only a small dependence on centrality until reaching more peripheral collisions, where the coeffiecient largely vanishes by the 60-70% centrality range.

B. Spectrum-weighted integral anisotropies.

The centrality dependence of the spectrum-weighted, integral v_n values are shown in Fig. 7 for the different methods. As noted for the $p_{\rm T}$-dependent results, the event-plane analysis for the higher harmonics ($n > 2$) using the event-plane order equal to that of the asymmetry harmonic have a weaker centrality dependence than that observed for elliptic flow. The v_4 behavior based on

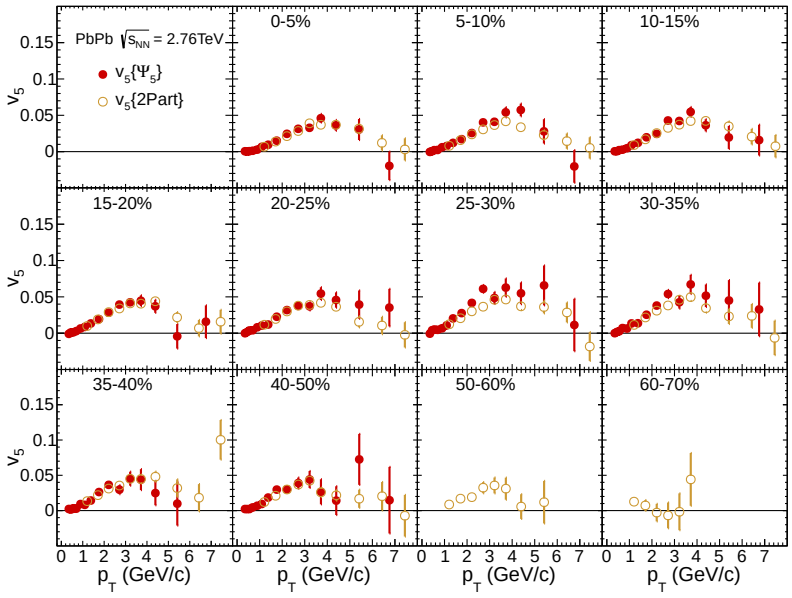

FIG. 6. (Color online) Azimuthal asymmetry v_5 coefficient for indicated methods.

TABLE IX. Summary of experimental conditions for the data shown in this report. The Figures column indicates the figures in this report where the data are shown. The p_T range for previously published data corresponds to that shown in the original report.

Method(s)	Figure(s)	Collaboration	η range	p_T range	Reference
$v_2\{\Psi_2\}$, $v_2\{4\}$, $v_2\{\text{LYZ}\}$	3	CMS	$\|\eta\| < 0.8$	0.3–20.0 GeV/c	[16]
$v_3\{\Psi_3\}$, $v_4\{\Psi_4\}$, $v_5\{\Psi_5\}$, $v_4\{\Psi_2\}$	3–6	CMS	$\|\eta\| < 0.8$	0.3–8.0 GeV/c	this report
$v_3\{4\}$	4	CMS	$\|\eta\| < 0.8$	0.3–4.0 GeV/c	this report
$v_4\{5\}$, $v_4\{\text{LYZ}\}$	5	CMS	$\|\eta\| < 0.8$	0.3–4.0 GeV/c	this report
$v_n\{\text{2Part}\}$	3–6	CMS	$\|\eta\| < 2.5; 2 < \|\Delta\eta\| < 4$	1.0–20 GeV/c	[44]
$v_2\{4\}$	7	ALICE	$\|\eta\| < 0.8$	0.2–5 GeV/c	[14]
$v_n\{\text{2Part}\}$	7–10	ALICE	$\|\eta\| < 1.0; \|\Delta\eta\| > 0.8$	0.25–15 GeV/c	[22]
$v_n\{\Psi_n\}$	7–10	ATLAS	$\|\eta\| < 2.5$	0.5–12 GeV/c	[24]

the second-order event plane increases from a small value for the most central events and reaches its maximum near 50% centrality, close to where maximum for the $v_2\{\Psi_2\}$ also occurs. The $v_4\{5\}$ and $v_4\{\text{LYZ}\}$ values are found to have similar dependence on centrality, altough with somewhat higher values for the Lee-Yang Zeros results.

Figure 8 shows the pseudorapidity dependence for the event-plane analyses of v_n. The data are sorted into ten pseudorapity bins of $\Delta\eta = 0.4$ spanning the range $-2.0 \leq \eta < 2.0$. The general behavior has the spatial anisotropy reaching its maximum value, with only a modest reduction going out two units of pseudorapidity. Both the v_2 and v_4 values based on the 2^{nd}-order event plane Ψ_2 show a much greater centrality dependence than observed for either the higher-order anistropies evaluated with the event-plane order (m) being the same as the order of the anisotropy (n).

C. Comparison with other results.

The current results extend and, in some cases, confirm previous results published by the ALICE [22, 23] and ATLAS [24] collaboration on higher-harmonic correlations. Representative comparisons of the CMS results with those of these other two collaborations are shown in Figures 9 to 12. Differences in the centrality and pseudorapidity ranges chosen by the different collaborations for reporting their results need to be considered in comparing the results. Table IX summarizes the experimental conditions for the diffrernent measurements.

Figure 9 compares results of the three experiments for the p_T-dependent v_3 coefficient. The ATLAS results for $v_3\{\Psi_3\}$ are consistently lower than the CMS results for all but the most periperal centality bin. This is expected based on the larger pseudorapidity range being used for the ATLAS measurement. Good agreement is seen between the two-particle correlation results of the CMS and

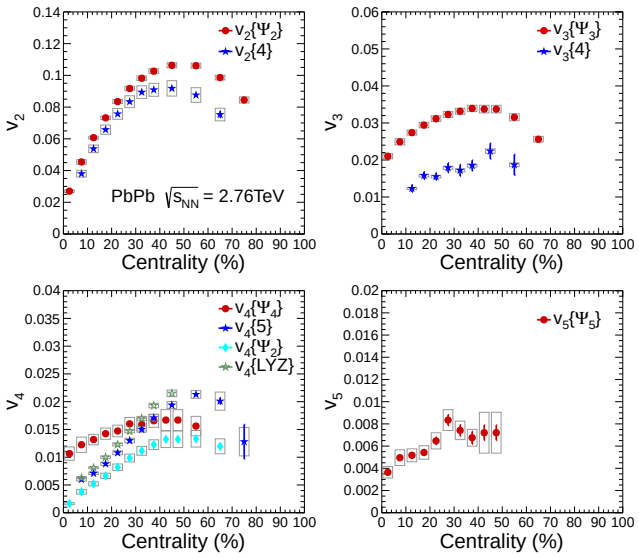

FIG. 7. (Color online) Centrality dependence of spectrum-weighted integral v_n coefficients with $0.3 \leq p_{\rm T} < 3.0$ GeV/c

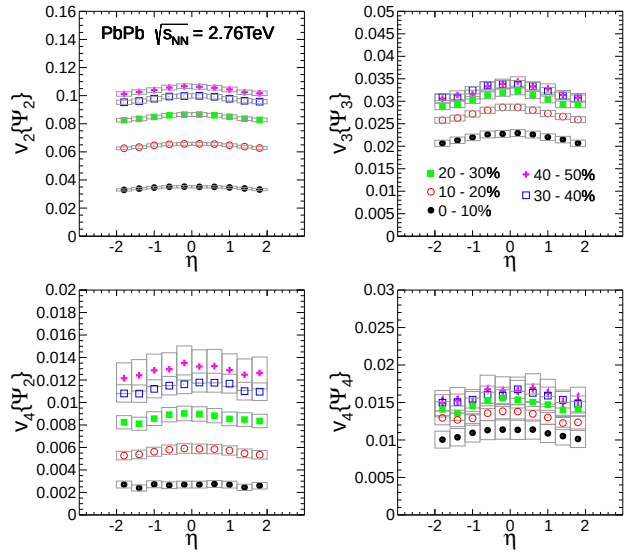

FIG. 8. (Color online) Pseudorapidity dependence of spectrum-weighted integral v_n coefficients with $0.3 \leq p_{\rm T} < 3.0$ GeV/c.

ALICE collaborations. This suggests that the pseudorapidity gap of $|\Delta\eta| > 0.8$ employed by ALICE is already sufficient to remove most of the di-jet contribution to these correlations. The comparison of v_4 (see Fig. 10) and v_5 (see Fig. 11) values found by the three experiments lead to similarly consistent results.

IV. DISCUSSION

There is considerable interest in the how the spatial anisotropies created early in the collision of two ultra-relativistic heavy ions and characterized by spatial asymmetry parameter ϵ_n gets transformed into the experimentally observerd azimuthal anisotropy of emitted particles [28, 32–34, 36, 37, 54–56]. The higher-harmonic anistotropies are particularly significant in their sensitivies to the initial state geometry. The odd harmonics are expected to arise entirely from fluctuations in the initial energy density, while higher order even harmonics will reflect both fluctuations and the influence of the initial state geometry. Recent theory calculations are exploring these effects on an event-by-event basis. The shear viscosity of the medium is also expected to influence the strength of the higher-harmonic terms in the azimuthal anistotropy [40, 42].

It is now recognized that the different experimental methods used in determining the v_n coefficient are related differently to the underlying ϵ_n. For example, $v_n\{\Psi_n\}$ values obtained with near-unity values for the event-plane resulution factor R are expected to scale with $\langle\epsilon_n\rangle$, whereas these values approach $\sqrt{\langle\epsilon_n^2\rangle}$ for lower values of R. The two-particle correlations are also expected to scale as $\sqrt{\langle\epsilon_n^2\rangle}$, whereas the $v_n\{4\}$ coefficient scales as the fourth order cumulant eccentricity.

The details of the eccentricity scaling is model dependent and beyond the scope of this paper. However, to achieve an overview of the scaled behavior, we present in Fig. 12 the spectrum-weighted integral v_n results of Fig. 7 scaled to the $\sqrt{\langle\epsilon_{n,m}^2\rangle}$ azimuthal asymmetries discussed in section II D. The $v_2/\sqrt{\langle\epsilon_2^2\rangle}$ ratio shows a steep falloff with centrality over most of the range from 10-80%, with a small decrease for the most central events. Similar behavor if observed for the $v_2\{4\}$ results, although with the cumulant results having a consistently smaller value. This offset is consistent with the 4^{th}-order cumulant result scaling with $\epsilon_2\{4\}$, except for the most central events, as shown in ref. [16].

The azimuthal anisotropy values for the higher order ($n > 2$) event-plane results with $n = m$ show an almost linear dependence with centrality, with similar slopes for the $n = 3$ and $n = 4$ anisotropies. The odd-harmonic $v_3\{4\}/\sqrt{\langle\epsilon_3^2\rangle}$ and $v_5\{\Psi_5\}/\sqrt{\langle\epsilon_5^2\rangle}$ results show only a weak centrality dependence, suggesting in these cases reasonably good scaling of the r.m.s. v_n values with the r.m.s. spatial anisotropies.

The $v_4\{5\}/\sqrt{\langle\epsilon_4^2\rangle}$, $v_4\{\rm LYZ\}/\sqrt{\langle\epsilon_4^2\rangle}$, and $v_4\{\Psi_2\}/\sqrt{\langle\epsilon_{4,2}^2\rangle}$ results all show a similar centrality dependence, with smaller values for more central and more peripheral centralities and maxima in the 30-50% centrality range. The very different behavior observed for these results compared to what is found for the odd harmonics coulds reflect the greater sensitivity of the v_4 coefficient to the initial overlap geometry. The

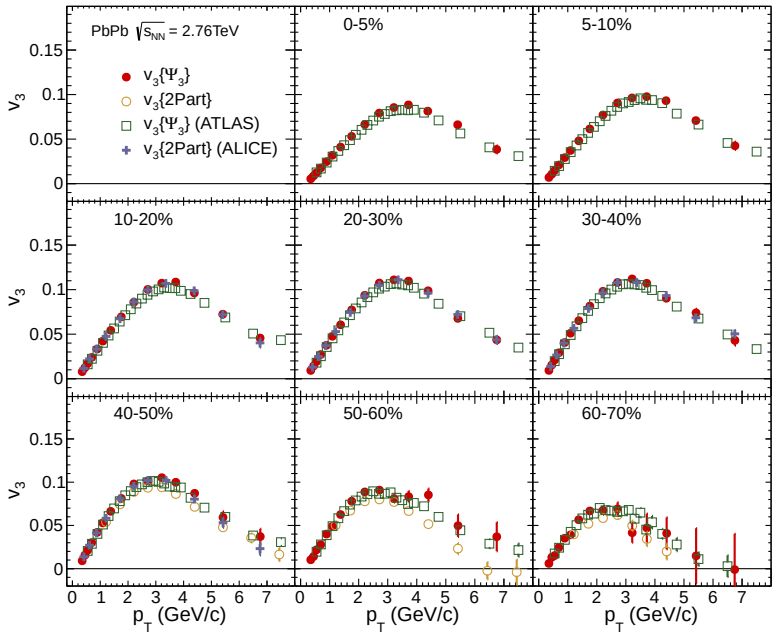

FIG. 9. (Color online) Comparison of the v_3 results of the ALICE, ATLAS and CMS collaborations. References given in Table IX.

.

lenticular shape of the overlap region for mid-central events is expected to require both v_2 and v_4 terms for its description [37].

Figure 13 shows the $v_n\{\Psi_n\}$ values as a function of the harmonic order n for five different $p_{\rm T}$ ranges and for four different centrality ranges. For all but the most central events, the v_n values are found to decrease with increasing harmonic number. The rate of this decrease is expected to be sensitive to the shear viscosity of the medium, which leads to greater damping of the higher harmonic anisotropies [42]. For the most central events, the v_3 coefficient is found to become larger than that for v_2 in range $1.6 \leq p_{\rm T} < 4.0$ GeV/c. This suggests the dominance of fluctuation effects for the most central collisions, where the spatial overlap assymetry would be expected to be small.

Figure 14 shows the same data as in Fig. 13, but scaled by the respective r.m.s. eccentricities. With this scaling, it is only the highest $p_{\rm T}$ range of $3.5 \leq p_{\rm T} < 4.0$ GeV/c shown in the figure where the v_3 component dominates over the other terms in the harmonic expansion. Otherwise, the trend is for a regular falloff of the scaled $v_n(p_{\rm T})$ values with harmonic number.

Considerable attention has been paid to the v_4/v_2^2 ratio [18, 20, 33, 42, 57–59] in characterizing the azimuthal anistropy. It is now reconized that the value of this ratio of 0.5, obtained through ideal hydrodynamics [58], is strongly affected by flow fluctuations and non-flow correlations and that comparisons of theory to the experimental results needs to account for how the results of the different analysis methods relate to the event-by-event v_n asymmetry [33]. Figure 15 shows the ratio $v_4\{\Psi_2\}/v_2^2\{\Psi_2\}$ for two different $p_{\rm T}$ ranges as a function of centrality. In both cases the ratio initially decreases, but then remains relatively constant for centralities greater than $\approx 20\%$. The ratio using the spectrum-weighted integral v_n values over the larger $p_{\rm T}$ range of $0.3 \leq p_{\rm T} < 3.0$ GeV/c tends is systematically larger than that found with the $p_{\rm T}$ range of $1.2 \leq p_{\rm T} < 1.6$ GeV/c. We also show the AuAu results obtained at $\sqrt{s_{NN}} = 200$ GeV/c by the PHENIX collaboration for the range $1.2 \leq p_{\rm T} < 1.6$ GeV/c. The CMS results are consistently higher. Although part of the difference between the PHENIX and CMS results could arise from the differences in the resolution parameters leading to the CMS v_2 results being closer to the average rather than the r.m.s. event-by-event v_2 values, this is unlikely to fully explain the difference since then we would expect a greater centrality dependence, reflecting the centrality dependence of R_2 (see Fig. 2).

V. CONCLUSIONS

We present the results of the CMS collaboration on higher-harmonic anisotropies of charged particle for PbPb collisions at $\sqrt{s_{NN}} = 2.76$ TeV. The harmonic v_n coefficients are studied as a function of transverse momentum, with $0.3 \leq p_{\rm T} < 8.0$ GeV/c, centrality (0-70%), and pseudorapdity ($-2.0 \leq \eta < 2.0$). Third-

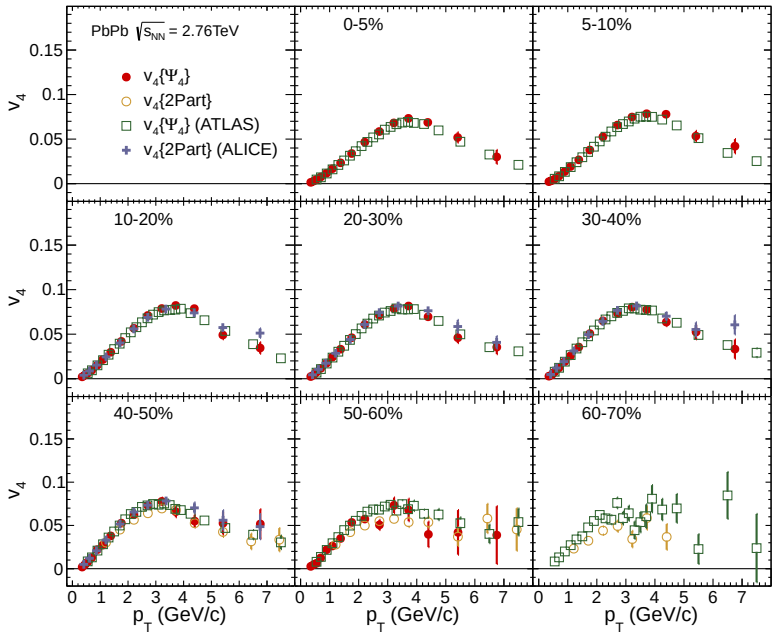

FIG. 10. (Color online) Comparison of the v_4 results of the ALICE, ATLAS and CMS collaborations. References given in Table IX.

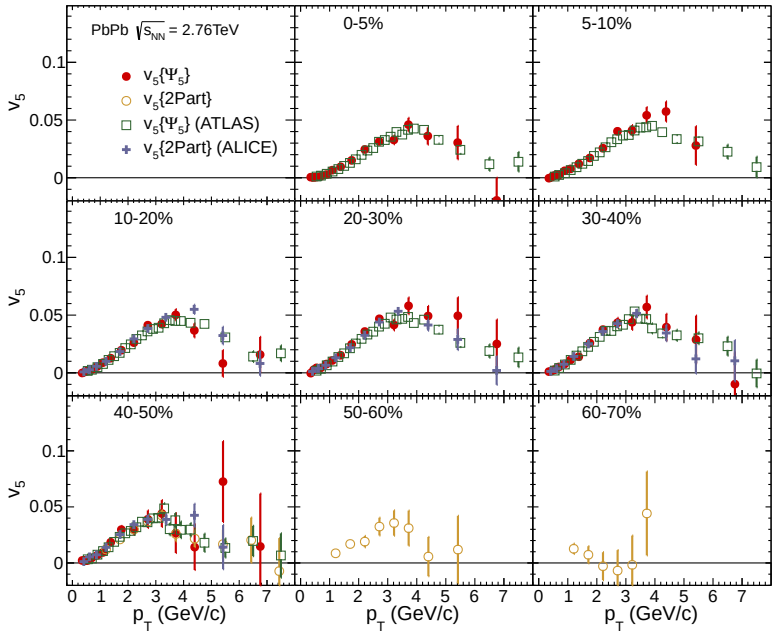

FIG. 11. (Color online) Comparison of the v_5 results of the ALICE, ATLAS and CMS collaborations. References given in Table IX.

harmonic v_3 coefficients are determined using the event-plane and four-particle cumulant methods. The event-plane results are obtained with a pseudorapidity gap of at least three units between the range for which the event plane is determined and any particle used for the asymmetry measurement, suppressing the contribution of non-flow contributions. The $v_3\{4\}$ are significantly smaller than found for the event-plane method, as expected for a initial-state fluctuation dominated asymmetry. Fourth-harmonic v_4 coefficents are found using the event plane

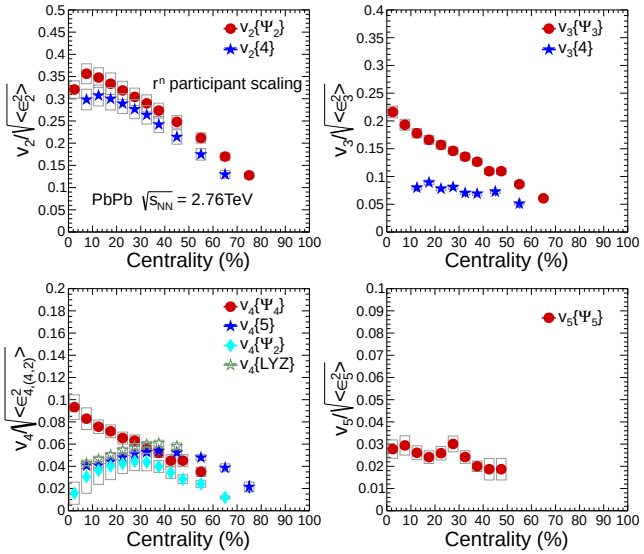

FIG. 12. (Color online) Spectrum-weighted integral results weighted by corresponding Glauber-model anisotropy parameters.

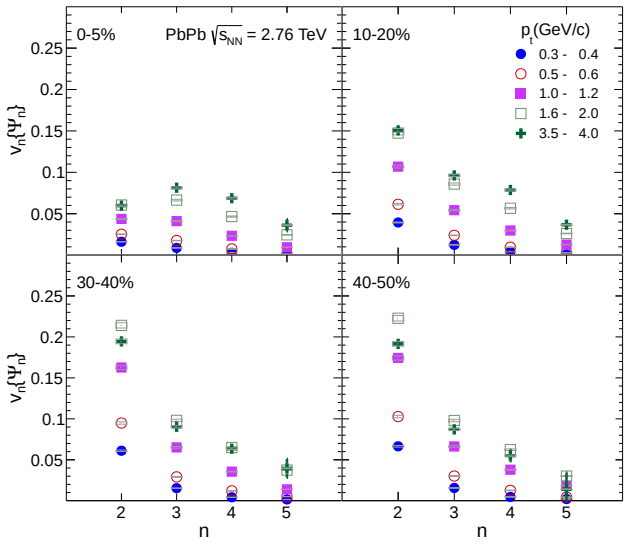

FIG. 13. (Color online) Order dependence of anisotropy parameter for indicated p_{T} ranges.

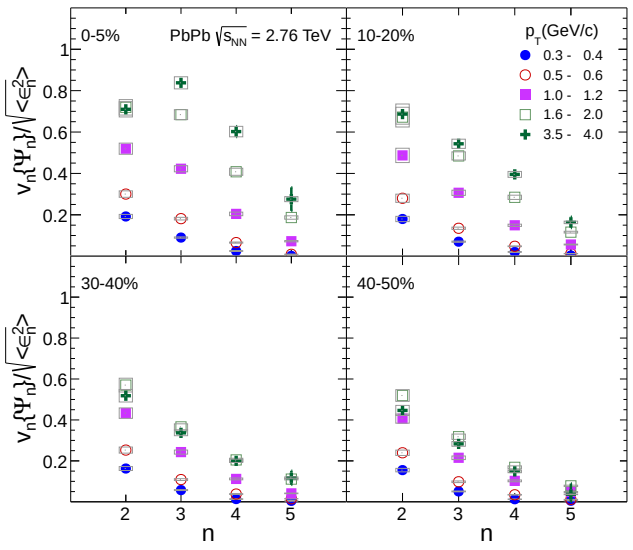

FIG. 14. (Color online) Order dependence of anisotropy parameter scaled by corresponding Glauber-model anisotropy for indicated p_{T} ranges.

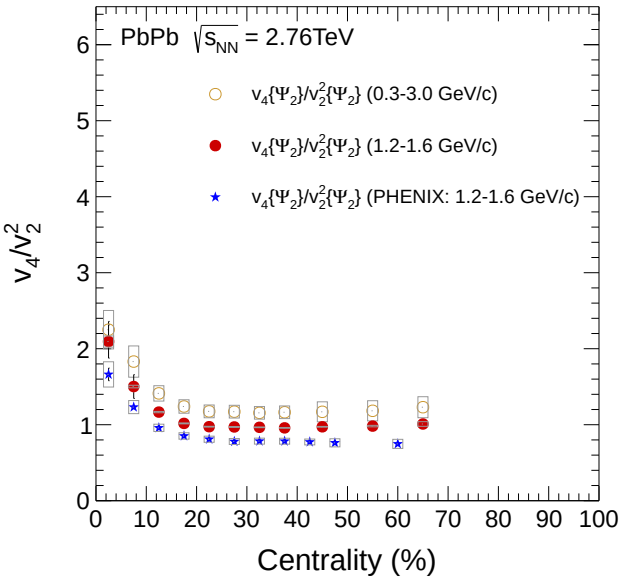

FIG. 15. (Color online) v_4/v_2^2 ratio. The PHENIX results are from ref. [20].

method (with a minimum three-unit pseudorapdity gap) based on both the 2^{nd} and 4^{th} order event planes, the five-particle cumulant method and the Lee-Yang Zeros method. For more central events ($<\approx 30\%$), the $v_4\{5\}$ and $v_4\{\mathrm{LYZ}\}$ results, which both involve the correlations of multiple particles, are again significantly smaller than found for $v_4\{\Psi_4\}$, consistent with a strong contribution of initial-state fluctuations to the asymmetry reasured with an event plane of the same order. For mid-rapidity and more peripheral collisions the multi-particle correlation methods result in v_4 coefficient similar in magnitude and, for the most peripheral collisions, larger than found for $v_4\{\Psi_4\}$. In contrast to the relativly flat $v_4\{\Psi_4\}$ centrality dependence, the $v_4\{\Psi_2\}$ values are very small for more central events, and then approach the $v_4\{\Psi_4\}$ values for more peripheral events. Finally, the fifth-harmonic v_5 term is found using the event-plane method. The pseudorapdity dependence of the higher-order azimuthal asym-

metry parameters based on the event plane method are similar to that observed for elliptic flow, with a maximum at midrapdity and a modest decrease out to the limits of the measurement at two units of pseudorapidity. The current results extend previously CMS results on elliptic flow v_2 [16] that were obtained under the same experimental coniditons and two-particle correlation results for v_2 through v_5 [44] covering a higher $p_{\rm T}$ range ($1.0 \leq p_{\rm T} < 20.0$ GeV/c). The CMS results are compared to those recently obtained by the ALICE [22, 23] and ATLAS [24] collaborations, and found to be in excellent agreement.

The r.m.s. eccentricity scaled v_n coefficients found using the same-order event-plane method are found to decrease monotonically for n=3,4,5. A similar behavior is observed for elliptic flow, although here the most central events also show a smaller eccentricy scaled value. The multi-particle correlation methods show a flatter centrality dependence for mid-central events, while the $v_4\{\Psi_2\}$ have a strong centrality dependence with a maximum in the 30-40% range, a somewhat smaller value than where the elliptic flow asymmetries reach their maximum values.

As a function of asymmetry harmonic number n, the $v_n\{\Psi_n\}(p_{\rm T})$ values decrease with increasing n, except for the most central events, where for $p_{\rm T}$ values above $\approx$ 1 GeV/c the asymmetry is greatest for $n = 3$. The r.m.s. eccentricity scaled results show similar behavior, altough the scaled values show less of a fall-off going to low-$p_{\rm T}$ values.

The data presented in this paper help to further establish the pattern of azimuthal particle emission at LHC energies. The results are directly applicable to the study of the initial spatial asymmetry, time development, and shear viscosity of the medium form in ultra-relativistic heavy-ion collisions. Athough a number of theory investigations have significantly increased our understanding of the initial conditions and hydrodynamics that lead to the experimentally observed asymmetry patterns, the method-dependent differences found for the flow harmonics emphasize the need for calculations that account for these differences.

[1] I. Arsene *et al.* (BRAHMS), Nuclear Physics A **757**, 1 (2005), arXiv:nucl-ex/0410020.
[2] B. B. Back *et al.* (PHOBOS), Nuclear Physics A **757**, 28 (2005), arXiv:nucl-ex/0410022.
[3] J. Adams *et al.* (STAR), Nuclear Physics A **757**, 102 (2005), arXiv:nucl-ex/0501009.
[4] K. Adcox *et al.* (PHENIX), Nuclear Physics A **757**, 184 (2005), arXiv:nucl-ex/0410003.
[5] M. Luzum and P. Romatschke, Physical Review C **78** (2008), arXiv:0804.4015 [nucl-th].
[6] S. Gavin and M. Abdel-Aziz, Physical Review Letters **97**, 162302 (2006), arXiv:nucl-th/0606061.
[7] A. Adare *et al.* (PHENIX), Physical Review Letters **98** (2007), arXiv:nucl-ex/0611018.
[8] H. J. Drescher, A. Dumitru, C. Gombeaud, and J. Y. Ollitrault, Physical Review C **76** (2007), arXiv:0704.3553 [nucl-th].
[9] J. Y. Ollitrault, Physical Review D **46**, 229 (1992).
[10] H. Sorge, Physical Review Letters **82**, 2048 (1999), arXiv:nucl-th/9812057.
[11] W. Reisdorf and H. G. Ritter, Annual Review of Nuclear and Particle Science **47**, 663 (1997).
[12] M. L. Miller, K. Reygers, S. J. Sanders, and P. Steinberg, Annual Review of Nuclear and Particle Science **57**, 205 (2007), arXiv:nucl-ex/0701025.
[13] L. D. McLerran, **583**, 291 (2002), arXiv:hep-ph/0104285.
[14] K. Aamodt *et al.* (ALICE), Physical Review Letters **105** (2010), arXiv:1011.3914 [nucl-ex].
[15] G. Aad *et al.* (ATLAS), Physics Letters B **707**, 330 (2012), arXiv:1108.6018 [hep-ex].
[16] S. Chatrchyan *et al.* (CMS), Physical Review C **87**, 014902 (2013), arXiv:1204.1409 [nucl-ex].
[17] J. Adams *et al.* (STAR), Physical Review C **72**, 014904 (2005), arXiv:nucl-ex/0409033.
[18] B. I. Abelev *et al.* (STAR), Physical Review C **75**, 054906 (2007), arXiv:nucl-ex/0701010.
[19] J. Adams *et al.* (STAR), Physical Review Letters **92**, 062301 (2004), arXiv:nucl-ex/0310029.
[20] A. Adare *et al.* (PHENIX), Physical Review Letters **105**, 062301 (2010), arXiv:1003.5586 [nucl-ex].
[21] A. Adare *et al.* (PHENIX), Physical Review Letters **107**, 252301 (2011), arXiv:1105.3928 [nucl-ex].
[22] K. Aamodt *et al.* (ALICE), Physics Letters B **708**, 249 (2012), arXiv:1109.2501 [nucl-ex].
[23] K. Aamodt *et al.* (ALICE), Physical Review Letters **107** (2011), arXiv:1105.3865 [nucl-ex].
[24] G. Aad *et al.* (ATLAS), Physical Review C **86**, 014907 (2012), arXiv:1203.3087 [hep-ex].
[25] A. M. Poskanzer and S. A. Voloshin, Physical Review C **58** (1998), arXiv:nucl-ex/9805001.
[26] B. Alver *et al.* (PHOBOS), Physical Review C **C81**, 034915 (2010), arXiv:1002.0534 [nucl-ex].
[27] B. Alver *et al.* (PHOBOS), Physical Review C **77** (2008), arXiv:0711.3724 [nucl-ex].
[28] B. Alver and G. Roland (PHOBOS), Physical Review C **C81**, 054905 (2010), arXiv:1003.0194 [nucl-th].
[29] B. H. Alver, C. Gombeaud, M. Luzum, and J. Y. Ollitrault, Physical Review C **82** (2010), arXiv:1007.5469 [nucl-th].
[30] R. S. Bhalerao and J. Y. Ollitrault, Physics Letters B **641**, 260 (2006), arXiv:nucl-th/0607009.
[31] W. Broniowski, P. Bozek, and M. Rubczynski, Physical Review C **76** (2007), arXiv:0706.4266 [nucl-th].
[32] S. Gavin and G. Moschelli, Physical Review C **85**, 014905 (2012), arXiv:1107.3317 [nucl-th].
[33] C. Gombeaud and J.-Y. Ollitrault, Physical Review C **81**, 014901 (2010), arXiv:0907.4664 [nucl-th].
[34] L. X. Han *et al.*, Physical Review C **84**, 064907 (2011), arXiv:1105.5415 [nucl-th].
[35] J.-Y. Ollitrault, A. M. Poskanzer, and S. A. Voloshin, Physical Review C **C80**, 014904 (2009), arXiv:0904.2315

[nucl-ex].
[36] G.-Y. Qin, H. Petersen, S. A. Bass, and B. Mller, Physical Review C **82**, 064903 (2010), arXiv:1009.1847 [PhysRevC.82.064903].
[37] Z. Qiu and U. Heinz, Physical Review C **84** (2011), arXiv:1104.0650 [nucl-th].
[38] S. A. Voloshin, (2006), arXiv:nucl-th/0606022.
[39] S. A. Voloshin, A. M. Poskanzer, A. Tang, and G. Wang, Physics Letters B **B659**, 537 (2008), arXiv:0708.0800 [nucl-th].
[40] B. Schenke, S. Jeon, and C. Gale, Physical Review Letters **106**, 042301 (2011), arXiv:1009.3244 [hep-ph].
[41] P. Staig and E. Shuryak, Physical Review C **84**, 044912 (2011), arXiv:1105.0676 [nucl-th].
[42] B. Schenke, S. Jeon, and C. Gale, Physical Review C **85**, 024901 (2012), arXiv:1109.6289 [hep-ph].
[43] M. Alvioli, H. Holopainen, K. J. Eskola, and M. Strikman, Physical Review C **85**, 034902 (2012), arXiv:1112.5306 [hep-ph].
[44] S. Chatrchyan *et al.* (CMS), Eur.Phys.J. **C72**, 2012 (2012), arXiv:1201.3158 [nucl-ex].
[45] S. Chatrchyan *et al.* (CMS), Journal of Instrumentation **3** (2008).
[46] O. Djuvsland and J. Nystrand, Physical Review C **83** (2011), arXiv:1011.4908 [hep-ph].
[47] W. Adam, B. Mangano, T. Speer, and T. Todorov, *Track reconstruction in the CMS tracker*, Tech. Rep. (2005).
[48] I. Lokhtin and A. Snigirev, European Physical Journal C **C45**, 211 (2006), arXiv:hep-ph/0506189.
[49] Z.-W. Lin *et al.*, Physical Review C **72**, 064901 (2005), arXiv:nucl-th/0411110.
[50] N. Borghini, P. M. Dinh, and J. Y. Ollitrault, Physical Review C **64** (2001), arXiv:nucl-th/0105040.
[51] N. Borghini, P. M. Dinh, and J.-Y. Ollitrault, (2001), arXiv:nucl-ex/0110016.
[52] R. S. Bhalerao, N. Borghini, and J. Y. Ollitrault, Nuclear Physics A **727**, 373 (2003), arXiv:nucl-th/0310016.
[53] N. Borghini, R. Bhalerao, and J. Ollitrault, **G30**, S1213 (2004), arXiv:nucl-th/0402053.
[54] R. S. Bhalerao, M. Luzum, and J. Y. Ollitrault, Physical Review C **84** (2011).
[55] R. A. Lacey *et al.*, Physical Review C **83**, 044902 (2011), arXiv:1009.5230 [nucl-ex].
[56] B. Schenke, P. Tribedy, and R. Venugopalan, Physical Review Letters **108**, 252301 (2012), arXiv:1202.6646 [nucl-th].
[57] P. F. Kolb, Physical Review C **68** (2003), arXiv:nucl-th/0306081.
[58] P. F. Kolb, L. W. Chen, V. Greco, and C. M. Ko, Physical Review C **69** (2004), arXiv:nucl-th/0402049.
[59] R. S. Bhalerao, J. P. Blaizot, N. Borghini, and J. Y. Ollitrault, Physics Letters B **627**, 49 (2005), arXiv:nucl-th/0508009.